Hindawi
Journal of Nanomaterials
Volume 2019, Article ID 5784610, 9 pages
https://doi.org/10.1155/2019/5784610

Research Article

Synthesis of $Bi_{0.5}Li_{0.5}TiO_3$ Nanoparticles by Sol-Gel Method for Photocatalytic Methylene Blue Degradation and Antibacterial Activity

Thanh T. Hai Le,[1,2] **Bao Quoc Phung**,[2] **and Dung Duc Dang**[1]

[1]*School of Engineering Physics, Hanoi University of Science and Technology, 1 Dai Co Viet Road, Hanoi, Vietnam*
[2]*Faculty of Physics, University of Science, Hanoi National University, 334 Nguyen Trai Road, Hanoi, Vietnam*

Correspondence should be addressed to Thanh T. Hai Le; lethihaithanh0609@gmail.com

Received 1 June 2019; Accepted 23 July 2019; Published 28 August 2019

Academic Editor: Oscar Perales-Pérez

Facile synthesis of nanomaterials for advanced characterization and application is gaining interest from many researchers. In this study, $Bi_{0.5}Li_{0.5}TiO_3$ nanoparticles were synthesized through the sol-gel method. The photocatalytic activity of the synthesized $Bi_{0.5}Li_{0.5}TiO_3$ was investigated for degradation of methylene blue (MB) under UV irradiation. A photocatalytic efficiency of 74% was found at 150 min when the degradation was performed in the basic media, and the kinetic rate constant was calculated equal to 0.0093 min^{-1}. The antibacterial activity of $Bi_{0.5}Li_{0.5}TiO_3$ nanoparticles was evaluated against *E. coli*, and the results showed considerable efficiency.

1. Introduction

Waste water discharged from the textile industry is considered a predominant source that generates organic pollutants, which cause severe problems to the environment in developing countries. Pollution is caused by organic dyes released during dyeing, which are not treated effectively before being discharged to the environment [1, 2]. Among the azo dyes widely used in the textile industry, methylene blue (MB) is a dye structured from aromatic amines that are highly carcinogenic [3]. Several methods are reported for the treatment of MB in wasted waters, such as adsorption, biodegradation, chemical treatment processes (ozonation and chlorination), micelle-enhanced ultrafiltration, and catalytic photodegradation [4–9]. Among these methods, the heterogeneous photocatalysis based on the generation of highly reactive radicals in the presence of a photocatalyst has been regarded as an effective alternative for MB degradation [10, 11]. Metal oxide-based photocatalysts have received considerable interest due to their technological effectiveness for eliminating environmental pollutions. Different materials such as Fe_2O_3, SnO_2, WO_3, ZnO, and TiO_2 have been used for the degradation of organic pollutants [12–14]. Among these metal oxides, TiO_2 is an effective photocatalyst for eliminating environmental contaminants because of its efficiency, affordability, and chemical stability [15]. For example, photocatalytic degradation of MB was achieved by a combination of TiO_2-anatase and coconut shell-activated carbon [16]. However, TiO_2 has a large band gap (3.2 eV), which requires ultraviolet illumination to activate, and a high electron-hole pair recombination rate, thus limiting its applications [17]. Therefore, semiconductor materials with suitable band gap and flat band potentials/energy levels to act as photocatalysts for the degradation of organic pollutants are deemed valuable and advantageous [18].

Recently, ABO_3 perovskite materials with higher surface areas suitable for catalytic and adsorption-related applications have been used as a new class of catalysts for the degradation of organic environmental pollutants [19]. Compared with other semiconductors, ABO_3 materials exhibit several advantages in photocatalysis due to their large scope to design, tunable band gap, and other photophysical properties attributed to the A and B cations [20]. $BaTiO_3$, $BiTiO_3$, and $BiFeO_3$, known as a class of ferroelectric materials, were also

considered in photocatalytic applications [21–25]. The use of $BiFeO_3/ZnFe_2O_4$ nanocomposites was reported for the photocatalytic degradation of organic dyes under visible light irradiation [26]. To improve the photocatalytic activity, doping at appropriate sites with suitable elements to control the optical properties and band gap of the perovskites has been an effective approach [27]. Methods based on conventional solid-state reaction require high sintering temperatures [28]; thus, efforts have been devoted to synthesize perovskites at lower temperatures. This method allows for high porosity remaining in the materials and thus induces advanced optical properties for an effectively photocatalytic degradation of organic dyes.

In this work, we put forward a sol-gel synthesis of $Bi_{0.5}Li_{0.5}TiO_3$ nanoparticles that can be used for the photocatalytic degradation of MB in water. This method poses the advantages of facile and fast synthesis, high loading yield of metal oxides, mass production, and prevention of magnetic nanoparticle aggregation. Effect of annealing temperatures on the morphology and structure of the nanoparticles was studied. In addition, photocatalytic activity was examined by kinetic experiments, and the antibacterial ability of the material was evaluated with *E. coli* samples.

2. Experimental

2.1. Chemicals. Bismuth nitrate pentahydrate ($Bi(NO_3)_3{\cdot}5H_2O$), lithium carbonate (Li_2CO_3), tetraisopropoxytitanium (IV) ($C_{12}H_{28}O_4Ti$), acetic acid (CH_3COOH), acetyl acetone ($CH_3COCH_2COCH_3$), and methylene blue (MB) were purchased from Sigma-Aldrich. All chemicals were of analytical grade and used without any further purifications.

2.2. Synthesis of $Bi_{0.5}Li_{0.5}TiO_3$ Nanoparticles. The $Bi_{0.5}Li_{0.5}TiO_3$ nanoparticles were synthesized through the sol-gel method [29]. $Bi(NO_3)_3{\cdot}5H_2O$ and Li_2CO_3 were dissolved in a mixture of acetic acid and distilled water (10 mL H_2O : 1 mL acetic acid) at room temperature. After stirring vigorously for 1 h, a transparent homogeneous sol was formed. Acetyl acetone was then introduced into the as-prepared solution after adding the tetraisopropoxytitanium (IV). The solutions were stirred for around 5 h at room temperature until a transparent solution was obtained. The transparent sol was then heated at 100°C to obtain dry gels. The dry gels were annealed at 400°C, 500°C, 600°C, and 700°C for 3 h in air before freely cooling down at room temperature. Lithium was added to excess around 180 mol% to prevent lithium loss during gel and calcining processes. The morphologies of the as-prepared materials were investigated using a field emission scanning electron microscopy (FE-SEM, JEOL model 6500). The crystal structures were studied by X-ray diffraction using a Bruker D8 Advance Diffractometer.

2.3. Photocatalytic Experiment. The photocatalytic performance of the synthesized $Bi_{0.5}Li_{0.5}TiO_3$ was evaluated by the degradation of MB dye under UV illumination from a source lamp of 254 nm, 400 W. The MB solution was prepared by dissolving it in water to obtain a concentration of 10^{-4} M (35.6 ppm). Initially, 20 mg of the photocatalyst was added to 40 mL of the MB solution. Before the UV illumination, the solution was stirred magnetically for 30 min in the darkness to achieve an adsorption-desorption equilibrium of the dye solution with catalyst. For every time interval of 30 min during the photocatalytic process, 4 mL of the suspension was collected and centrifuged, and MB concentration was determined by using a spectrophotometer (UV-VIS, Optima SP-3000-nano, Japan). Beer-Lambert's law was used to express the calibration plots for relationship of the absorbance and concentration. The photocatalytic activity was investigated at different pH values, such as 3, 6.5, and 9, that were adjusted using either NaOH or HNO_3.

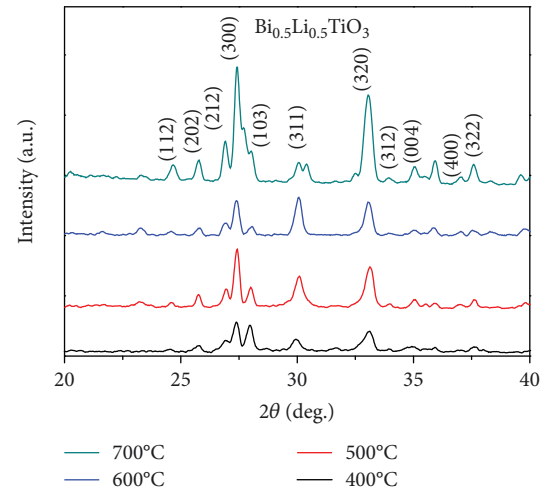

FIGURE 1: X-ray diffraction of $Bi_{0.5}Li_{0.5}TiO_3$ samples calcined at different temperatures.

2.4. Antibacterial Activity. The antibacterial activity against *E. coli* of $Bi_{0.5}Li_{0.5}TiO_3$ was investigated using the colony-counting method [30]. Two different concentrations of $Bi_{0.5}Li_{0.5}TiO_3$, 15 and 50 mg/mL, were used to evaluate the influence of the catalyst concentration to the antibacterial activity. The samples were taken out at 6, 12, 24, and 48 h for measuring the average concentration of bacteria.

3. Results and Discussion

3.1. Material Characteristics. The effect of calcination temperature on crystalline characteristics of $Bi_{0.5}Li_{0.5}TiO_3$ was investigated by X-ray diffraction as shown in Figure 1. The diffraction peaks at 24.6°, 25.4°, 25.8°, 27.0°, 27.4°, 28.0°, 30.3°, 33.1°, 34.1°, 35.5°, 36.9°, and 37.7° appeared on all samples in the range of 400–700°C. These peaks were attributed to the single phase of $Bi_{0.5}Li_{0.5}TiO_3$ [31]. In the case of the calcination temperature at 700°C, a peak occurred at 31.1°, which can assign the $Bi_2Ti_2O_7$ impurity phase, as mentioned in our previous work [26]. No peak on $Bi_2Ti_2O_7$ was observed when the calcination temperature was in the range of 400°C to 600°C. In addition, the increase of calcination temperature leads to the increasing height of diffraction peaks and the decreasing full width at half maximum. This

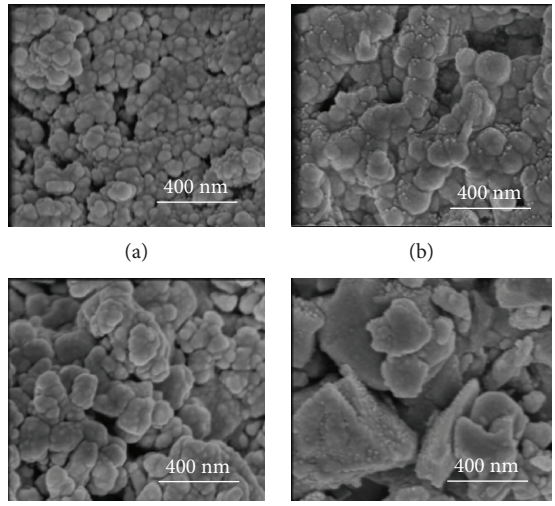

FIGURE 2: SEM images of $Bi_{0.5}Li_{0.5}TiO_3$ nanoparticles calcined at different temperatures: (a) 400°C, (b) 500°C, (c) 600°C, and (d) 700°C.

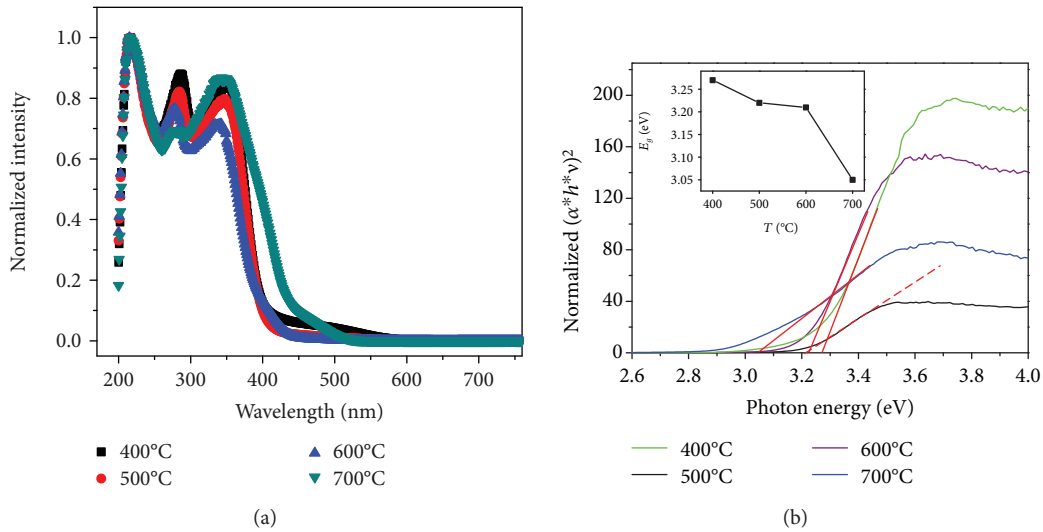

FIGURE 3: (a) UV-vis spectra of $Bi_{0.5}Li_{0.5}TiO_3$ powders calcined at different temperatures; (b) the optical band gap estimated by the Wood and Tauc method. The inset shows that optical band gap values depended on the calcination temperature.

phenomenon showed that crystal growth and the size of grains were improved when calcination temperature was increased.

Surface morphologies of $Bi_{0.5}Li_{0.5}TiO_3$ powders calcined at different temperatures were observed by FE-SEM, as shown in Figure 2. $Bi_{0.5}Li_{0.5}TiO_3$ grains are nearly spherical in shape, and their diameters increase when the calcination temperature is increased. Adjusting the calcination temperature from 400°C to 600°C leads to the increase of grain diameters from 50 nm to 200 nm. This result is consistent with the tendency of increasing grain size as mentioned in X-ray diffraction.

The optical properties of $Bi_{0.5}Li_{0.5}TiO_3$, including absorption spectra and optical band gap, are shown in Figure 3. Figure 3(a) indicates that $Bi_{0.5}Li_{0.5}TiO_3$ samples are strongly absorbed in the range of UV light from 200 to 450 nm. No considerable differences on the absorption bands are observed when the calcination temperature is adjusted from 400°C to 600°C. However, a slight shift of the absorption band towards a longer wavelength is observed at the sample calcined at 700°C. This finding seems to relate with the appearance of the $Bi_2Ti_2O_7$ impurity phase at the calcination temperature of 700°C.

The optical bandgap energy, E_g, was extracted by the Wood and Tauc method [32]. This method suggested that the optical band gap is related to the absorbance and photon energy through the following equation:

$$\alpha \cdot h \cdot \nu = c\left(h \cdot \nu - E_g\right)^n, \quad (1)$$

where α is the absorbance coefficient, h is the Planck constant, ν is the light frequency, and n is a constant depending on different types of electron transition ($n = 1/2$ for direct

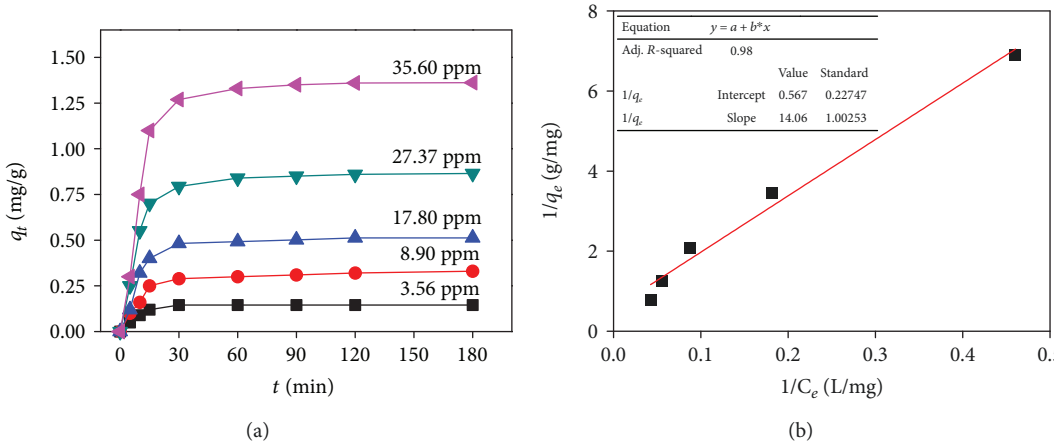

FIGURE 4: (a) Kinetics of the MB adsorption on $Bi_{0.5}Li_{0.5}TiO_3$ and (b) Langmuirian linear transform.

allowed transition, $n = 2$ for indirect allowed transition, $n = 3/2$ for the direct forbidden transition, and $n = 3$ for the indirect forbidden transition [32]). By plotting a graph of $(\alpha \cdot h \cdot \nu)^{1/n}$ versus $h \cdot \nu$, a straight line can be subsequently obtained. This line intersects the x-axis at $(\alpha \cdot h \cdot \nu)^{1/n} = 0$, and the value of E_g can be estimated from this intercept. Figure 3(b) shows the plots of $(\alpha \cdot h \cdot \nu)^2$ versus $h \cdot \nu$ for the $Bi_{0.5}Li_{0.5}TiO_3$ samples calcined at different calcination temperatures in the range of 400°–700°C. The Figure 3(b) inset also indicates that the band gap reaches the highest value of 3.27 eV on the sample calcined at 400°C, whereas the lowest value of 3.05 eV is found on the sample calcined at 700°C. The $Bi_{0.5}Li_{0.5}TiO_3$ material's band gap value can be considered as the structural order-disorder of the lattice caused by the symmetry disruption of the O–Ti–O bonds and the distortion of the TiO_6 clusters [33]. Calcination at a low temperature is not sufficient in reducing the defects into the $Bi_{0.5}Li_{0.5}TiO_3$ lattice, thereby leading to its high band gap value. Increasing the calcination temperature results in the reduction of defect density in the lattice and increase in crystalline size. These two factors explain the decrease of the band gap values with respect to the increase in calcination temperature. Moreover, the lowest band gap value found at the calcination temperature of 700°C can be caused by the impurity phase.

As previously mentioned, the sample calcined at 700°C appears with a $Bi_2Ti_2O_7$ impurity phase, whereas the sample calcined at 400°C exhibits the highest band gap value compared with other samples. In addition, no considerable differences of other properties were found between the two samples calcined at 500°C and 600°C, so $Bi_{0.5}Li_{0.5}TiO_3$ calcined at 500°C was chosen to investigate photocatalytic activity.

3.2. Photocatalytic Degradation of Methylene Blue by $Bi_{0.5}Li_{0.5}TiO_3$/UV

3.2.1. Adsorption of Methylene Blue by $Bi_{0.5}Li_{0.5}TiO_3$. The kinetics of the MB adsorption in the darkness for various initial concentrations, C_0, within the range of 3.56–35.6 ppm is illustrated in Figure 4(a). The quantities given in mg/g_{cat} of the adsorbed MB at the time t, q_t, were defined by the following equation:

$$q_t = \frac{(C_0 - C_t) \cdot V}{m_{\text{cat}}}, \tag{2}$$

where C_t is the MB concentration in the solution at time t defined through the UV-vis method (mg·L^{-1}), V is the volume of the solution (in L), and m_{cat} is the mass of $Bi_{0.5}Li_{0.5}TiO_3$.

The steady state of adsorption is reached within 30 min for all the initial concentrations. Thus, this time was selected as the least adsorption time before UV irradiation in the degradation experiments.

The kinetics of the MB adsorption are considered according to the Langmuir model by the following equation:

$$\frac{1}{q_e} = \frac{1}{K_L q_m} \cdot \frac{1}{C_e} + \frac{1}{q_m}, \tag{3}$$

where q_e and C_e are the quantities of the adsorbed MB and its concentration in the solution at the equilibrium time, respectively. q_m is the maximum quantities, and K_L is the adsorption constant. From the data in Figure 4(a), a linear transform of equation (2) can be determined by plotting $(1/q_e)$ as a function of $1/C_e$, as shown in Figure 4(b). The linearity of the transform is exhibited by a correlation coefficient R^2, with a value of 0.988. It indicates that the Langmuir isotherm is correctly observed and implies a monolayer adsorption model. From the slope and the intercept value of the linear line, q_m of 1.7630 mg·g^{-1} and K_L of 0.0403 L·mg^{-1} can be calculated.

3.2.2. Photocatalytic Degradation of Methylene Blue by $Bi_{0.5}Li_{0.5}TiO_3$. The photocatalytic activity of the as-synthesized $Bi_{0.5}Li_{0.5}TiO_3$ was investigated for the degradation of MB under the UV irradiation. Figure 5(a) shows the change in the UV-vis absorbance spectra of the MB solution during the degradation in the presence of $Bi_{0.5}Li_{0.5}TiO_3$ as a

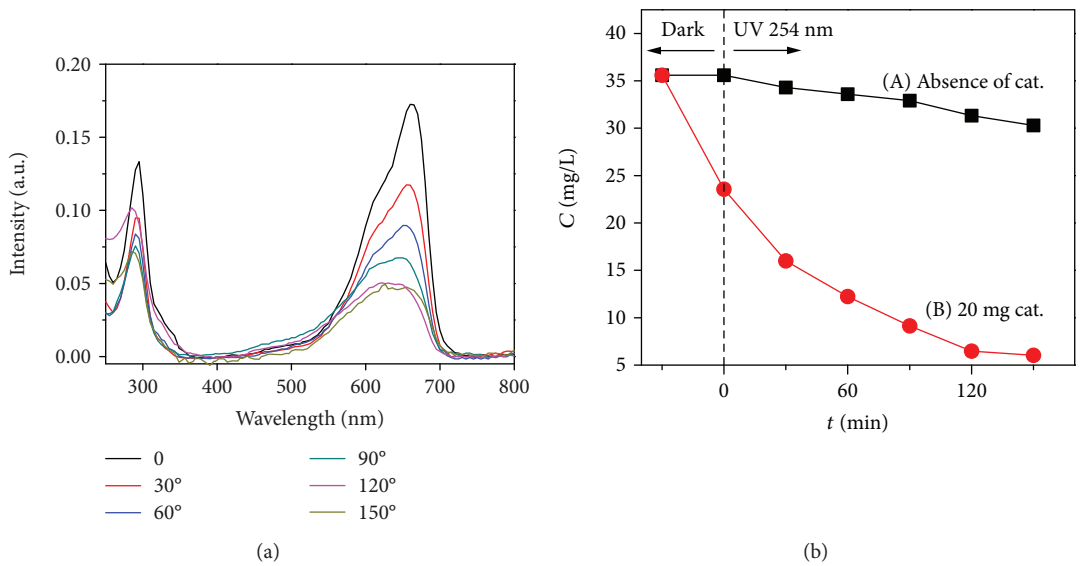

FIGURE 5: (a) MB absorbance at different time intervals during the photocatalytic degradation; (b) changes in the concentration of the MB by photochemistry and photocatalysis under UV irradiation at $\lambda = 254$ nm.

catalyst. As the UV-vis absorbance spectra, the MB solution exhibits two absorption peaks at 290 nm and 650 nm, wherein the amplitude of the 650 nm peak drops steadily with the increasing reaction time. This finding indicates that the degradation of MB occurs under the effect of the UV irradiation and of the $Bi_{0.5}Li_{0.5}TiO_3$ material. To demonstrate the catalyst's role, an experiment was performed in the absence of $Bi_{0.5}Li_{0.5}TiO_3$ which is known as the direct photolysis. The changes of MB concentration extracted from the absorbance spectra are shown in Figure 5(b). Evidently, change in the MB concentrations caused by the photolysis (line A) is negligible during the UV irradiation compared with the photocatalysis method (line B). Thus, $Bi_{0.5}Li_{0.5}TiO_3$ plays an apparent role as a photocatalyst for MB degradation.

The kinetics of the disappearance of MB is exhibited in Figure 5(b) (line B), in which MB adsorption in the dark was made 30 min before performing UV irradiation. The efficiency of degradation of the dye (D%) was determined by the following equation:

$$D\% = \frac{(C_{0a} - C_t)100}{C_{0a}}, \quad (4)$$

where C_{0a} and C_t are the concentrations at equilibrium adsorption ($t = 0$) and time t, respectively. The data in Figure 5(b) indicate that the efficiency of MB degradation by photocatalysis reaches 74% at 150 min. The kinetic mechanism of MB degradation is investigated by using the Langmuir-Hinshelwood model that is expressed by the following kinetic equation [33–35]:

$$\ln(C_{0a}/C_t) = K_{app} \cdot t + \text{constant}, \quad (5)$$

where K_{app} is the first-order catalytic rate constant.

The linear transform $\ln(C_{0a}/C_t) = f(t)$, shown in Figure 6, indicates that the Langmuir-Hinshelwood mechanism is

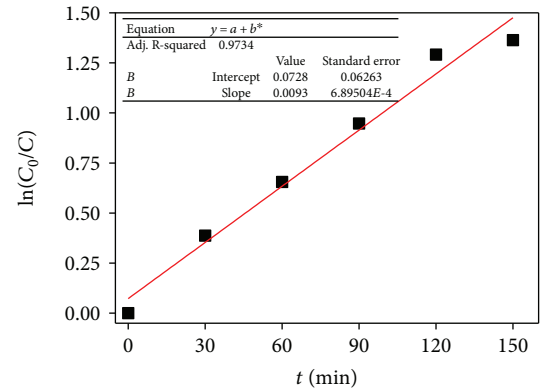

FIGURE 6: First-order kinetics of the degradation of MB by the photocatalysis under UV irradiation at $\lambda = 254$ nm.

appropriate for the MB dye degradation with the $Bi_{0.5}Li_{0.5}TiO_3$ photocatalyst. The calculated K_{app} from the slope of the linear line was 0.0093 min^{-1}.

3.2.3. Influence of pH. MB dye is considered a cationic chromophore, so its absorbance and degradation depend on pH. To investigate the influence of pH to MB degradation by the $Bi_{0.5}Li_{0.5}TiO_3$ photocatalyst, experiments were conducted at different pH values, such as 3, 6.5, and 9. Figure 7(a) shows the changes of the MB concentration during the reaction time corresponding to the mentioned pH values. At time $t = 0$, the adsorbed MB concentration increases with pH, whereas the degradation is improved when using the basic media. The fact that the basic media increases the density of the hydroxyl group (–OH) on the $Bi_{0.5}Li_{0.5}TiO_3$ surface and favors the generation of the *OH radicals can further explain this finding [34]. Therefore, the basic media directly improves the photocatalytic degradation of the MB dye.

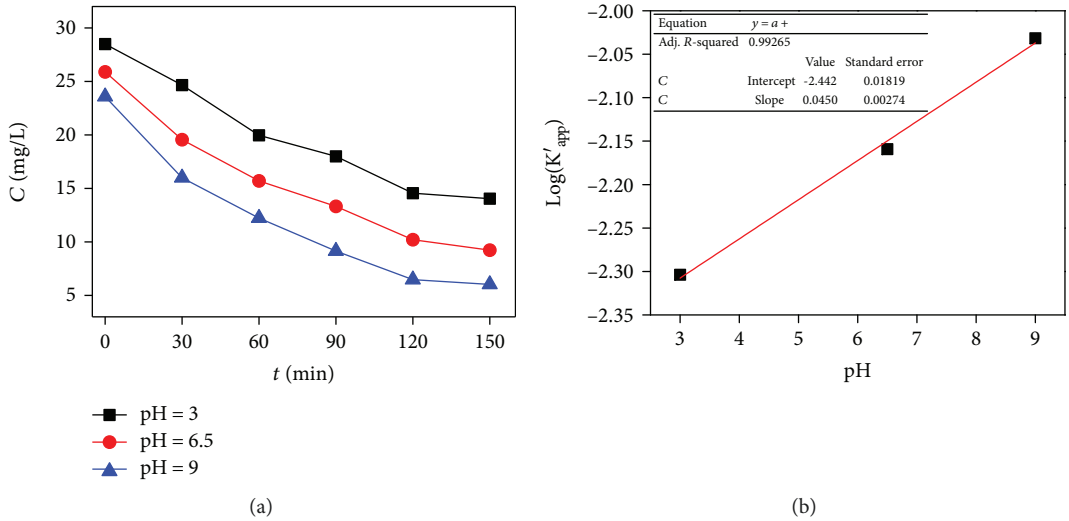

FIGURE 7: (a) Influence of pH to kinetics of MB degradation; (b) the plot of log $K'_{app} = f(\text{pH})$. Experimental conditions: $C_0 = 35.6$ mg/L, $m(Bi_{0.5}Li_{0.5}TiO_3) = 20$ mg, and $V = 40$ mL.

A method based on the kinetic partial order [34, 35] was used to investigate the influence of pH on the photocatalytic degradation that is expressed by the following equation:

$$\text{Log}r = \log K'_{app} - n\text{pH}, \quad (6)$$

where r is the reaction rate, K'_{app} is the pH-independent apparent rate constant, and n is the kinetic partial order with respect to the H^+ concentration. The result is shown under the linear transform $\log(K'_{app}) = f(\text{pH})$ in Figure 7(b). The slope is found at +0.045, which means that the kinetic partial order $n < 0.1$ in absolute value. Furthermore, protons (H^+) do not significantly influence the rate limiting step of the photocatalytic degradation. Thus, pH does not directly influence the Langmuir-Hinshelwood mechanism.

3.2.4. Influence of Scavengers. To estimate the effect of the active species on $Bi_{0.5}Li_{0.5}TiO_3$ to MB degradation, experiments were made in the presence of different scavengers, such as isopropyl alcohol (IPA), benzoquinone (BQ), and ethylenediaminetetraacetic acid (EDTA), to capture $^*OH$, $^*O_2^-$, and holes, respectively [36]. Figure 8 shows the change of the C/C_0 ratio during the UV irradiation corresponding to scavengers.

At time $t = 150$ min, the absence of any scavenger ("no scavenger") gives the highest degradation efficiency at 74%. In the presence of BQ and EDTA, the MB dye degradation is reduced slightly to 57% and 65%, respectively. The lowest efficiency is found at 28% in the presence of IPA. These results show that the $^*OH$ species play the most important role in the photocatalysis using $Bi_{0.5}Li_{0.5}TiO_3$. This finding is similar with the influence of pH as mentioned above.

3.3. Antibacterial Activity of $Bi_{0.5}Li_{0.5}TiO_3$. The antibacterial activity of $Bi_{0.5}Li_{0.5}TiO_3$ against *E. coli* was evaluated using the colony-counting method. The tests were performed with two different concentrations of $Bi_{0.5}Li_{0.5}TiO_3$, which are 15

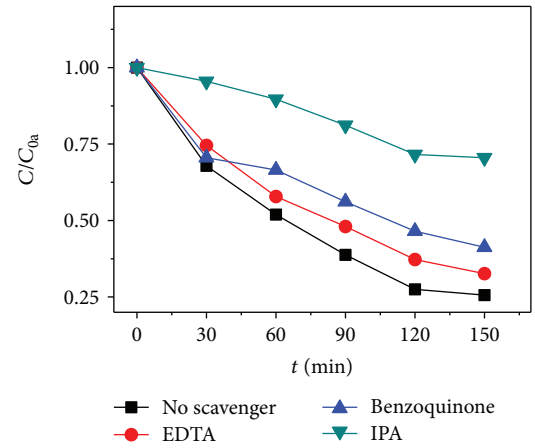

FIGURE 8: Influence of scavengers to the photocatalytic degradation of MB by $Bi_{0.5}Li_{0.5}TiO_3$. Experimental conditions: $C_0 = 35.6$ mg/L, $m(Bi_{0.5}Li_{0.5}TiO_3) = 20$ mg, and $V = 40$ mL.

and 50 mg/mL. The results are illustrated in Figure 9. As observed in Figure 9, the number of *E. coli* colonies decreases while the time increases from 0 h (Figure 9(a)) to 48 h (Figure 9(c)), thereby indicating that $Bi_{0.5}Li_{0.5}TiO_3$ at 15 mg/mL has considerable antibacterial activity against *E. coli*. This result is clearly shown in the plot on Figure 9(e) (black line); that is, the average concentration of *E. coli* decreases quickly from 10^8 to 2×10^7 CFU/mL during the 12 h initial time and reaches 10^7 CFU/mL at 48 h.

When the $Bi_{0.5}Li_{0.5}TiO_3$ catalyst is used at 50 mg/mL, *E. coli* colonies nearly disappear at initial time $t = 6$ h (Figure 9(d)), which found a concentration of 10^2 CFU/mL (Figure 9(e), red line). Thus, the antibacterial efficiency increases significantly with the catalyst concentration. The antibacterial activity of the photocatalytic materials is concerned with the destruction of the cell membrane [37]. Furthermore, the photocatalytic activity of the $Bi_{0.5}Li_{0.5}TiO_3$

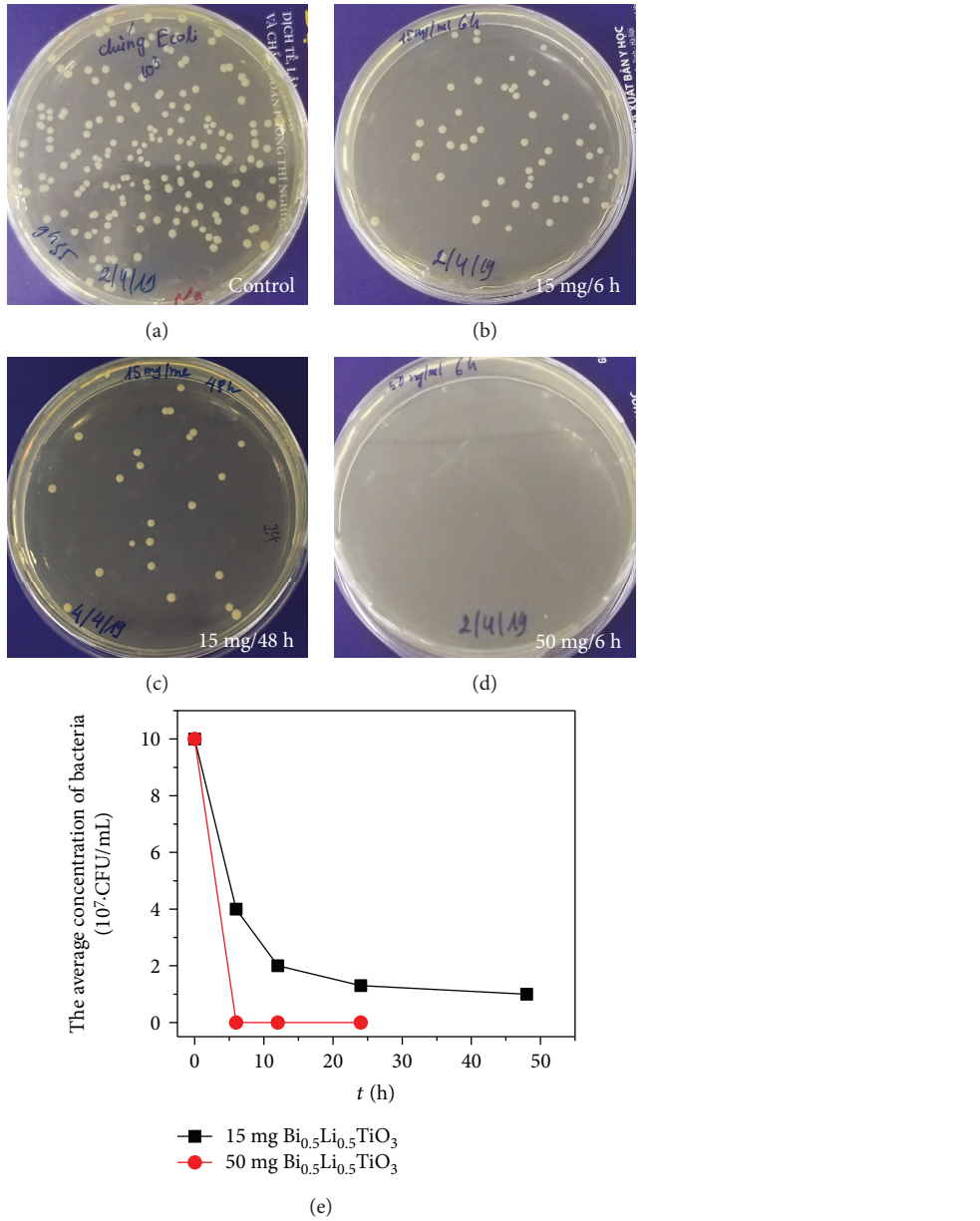

FIGURE 9: Changes of *E. coli* colonies: (a) without catalyst; (b, c) in the presence of a 15 mg/mL catalyst during 6 h and 48 h, respectively; (d) in the presence of a 50 mg/mL catalyst during 6 h; (e) antibacterial activity of $Bi_{0.5}Li_{0.5}TiO_3$ catalyst.

material seems to cause a degradation of the organic composition on the cell membrane under the visible light and consequently leads to cell death. These results show that the $Bi_{0.5}Li_{0.5}TiO_3$-based catalyst is an effective material for waste water antimicrobial performance.

4. Conclusion

In this work, the $Bi_{0.5}Li_{0.5}TiO_3$ material was synthesized by the sol-gel method that exhibits fast production, high loading yield of metal oxides, and prevention of magnetic nanoparticle aggregation. The material adsorbed strongly in a broad band of the UV light. The photocatalytic investigation with MB dye in UV irradiation showed that the Langmuir isotherm is an appropriate mechanism for absorption and that the Langmuir-Hinshelwood model is an effective pattern for degradation. Moreover, the photocatalytic activity of $Bi_{0.5}Li_{0.5}TiO_3$ significantly improved when used in the basic media. The $Bi_{0.5}Li_{0.5}TiO_3$-based catalyst was tested in antibacterial experiments and showed considerable effectiveness in the growth reduction of *E. coli*.

Data Availability

The data used to support the findings of this study are included within the article.

Conflicts of Interest

The authors declare that they have no conflicts of interest.

Acknowledgments

This research was funded by the Hanoi University of Science and Technology under project number T2017-PC-131.

References

[1] T. V. Luong, S. Schmidt, S. A. Deowan, J. Hoinkis, A. Figoli, and F. Galiano, "Membrane bioreactor and promising application for textile industry in Vietnam," *Procedia CIRP*, vol. 40, pp. 419–424, 2016.

[2] F. Azeez, E. al-Hetlani, M. Arafa et al., "The effect of surface charge on photocatalytic degradation of methylene blue dye using chargeable titania nanoparticles," *Scientific Reports*, vol. 8, no. 1, 2018.

[3] V. Vadivelan and K. V. Kumar, "Equilibrium, kinetics, mechanism, and process design for the sorption of methylene blue onto rice husk," *Journal of Colloid and Interface Science*, vol. 286, no. 1, pp. 90–100, 2005.

[4] W. Z. Tang and H. An, "UV/TiO2 photocatalytic oxidation of commercial dyes in aqueous solutions," *Chemosphere*, vol. 31, no. 9, pp. 4157–4170, 1995.

[5] M. Bielska and J. Szymanowski, "Removal of methylene blue from waste water using micellar enhanced ultrafiltration," *Water Research*, vol. 40, no. 5, pp. 1027–1033, 2006.

[6] G. Ciardelli and N. Ranieri, "The treatment and reuse of wastewater in the textile industry by means of ozonation and electroflocculation," *Water Research*, vol. 35, no. 2, pp. 567–572, 2001.

[7] L. Ai and J. Jiang, "Removal of methylene blue from aqueous solution with self-assembled cylindrical graphene–carbon nanotube hybrid," *Chemical Engineering Journal*, vol. 192, pp. 156–163, 2012.

[8] S. Chatterjee, A. Kumar, S. Basu, and S. Dutta, "Application of response surface methodology for methylene blue dye removal from aqueous solution using low cost adsorbent," *Chemical Engineering Journal*, vol. 181-182, pp. 289–299, 2012.

[9] M. Ghaedi, M. Pakniat, Z. Mahmoudi, S. Hajati, R. Sahraei, and A. Daneshfar, "Synthesis of nickel sulfide nanoparticles loaded on activated carbon as a novel adsorbent for the competitive removal of methylene blue and safranin-O," *Spectrochimica Acta Part A: Molecular and Biomolecular Spectroscopy*, vol. 123, pp. 402–409, 2014.

[10] A. Benzaouak, I. Ellouzi, F. Ouanji et al., "Photocatalytic degradation of methylene blue (MB) dye in aqueous solution by ferroelectric $Li_{1-x}Ta_{1-x}W_xO_3$ materials," *Colloids and Surfaces A: Physicochemical and Engineering Aspects*, vol. 553, pp. 586–592, 2018.

[11] J. Lin, Z. Luo, J. Liu, and P. Li, "Photocatalytic degradation of methylene blue in aqueous solution by using ZnO-SnO 2 nanocomposites," *Materials Science in Semiconductor Processing*, vol. 87, no. 20, pp. 24–31, 2018.

[12] S. Li, Q. Lin, X. Liu et al., "Fast photocatalytic degradation of dyes using low- power laser-fabricated Cu_2O–Cu nanocomposites," *RSC Advances*, vol. 8, no. 36, pp. 20277–20286, 2018.

[13] R. B. Anjaneyulu, B. S. Mohan, G. P. Naidu, and R. Muralikrishna, "Visible light enhanced photocatalytic degradation of methylene blue by ternary nanocomposite, MoO_3/Fe_2O_3/rGO," *Journal of Asian Ceramic Societies*, vol. 6, no. 3, pp. 183–195, 2018.

[14] V. T. Pham, H. le Trung, N. K. Tran et al., "Hydrothermal synthesis, structure, and photocatalytic properties of SnO_2/rGO nanocomposites with different GO concentrations," *Materials Research Express*, vol. 5, no. 9, 2018.

[15] C. Xu, G. P. Rangaiah, and X. S. Zhao, "Photocatalytic degradation of methylene blue by titanium dioxide: experimental and modeling study," *Industrial & Engineering Chemistry Research*, vol. 53, no. 38, pp. 14641–14649, 2014.

[16] H. A. Le, L. T. Linh, S. Chin, and J. Jurng, "Photocatalytic degradation of methylene blue by a combination of TiO_2-anatase and coconut shell activated carbon," *Powder Technology*, vol. 225, pp. 167–175, 2012.

[17] R. S. Dariani, A. Esmaeili, A. Mortezaali, and S. Dehghanpour, "Photocatalytic reaction and degradation of methylene blue on TiO_2 nano-sized particles," *Optik*, vol. 127, no. 18, pp. 7143–7154, 2016.

[18] R. J. Tayade, T. S. Natarajan, and H. C. Bajaj, "Photocatalytic degradation of methylene blue dye using ultraviolet light emitting diodes," *Industrial and Engineering Chemistry Research*, vol. 48, no. 23, pp. 10262–10267, 2009.

[19] N. Labhasetwar, G. Saravanan, S. Kumar Megarajan et al., "Perovskite-type catalytic materials for environmental applications," *Science and Technology of Advanced Materials*, vol. 16, no. 3, pp. 036002–036013, 2015.

[20] P. Kanhere and Z. Chen, "A review on visible light active perovskite-based photocatalysts," *Molecules*, vol. 19, no. 12, pp. 19995–20022, 2014.

[21] M. Rawat and K. L. Yadav, "Compositional effects on structural, dielectric, ferroelectric and transport properties of $Ba_{1-x}(Bi_{0.5}Li_{0.5})_xTiO_3$ ceramics," *Materials Chemistry and Physics*, vol. 148, no. 3, pp. 655–663, 2014.

[22] S. Ramakanth and K. C. J. Raju, "Band gap narrowing in BaTiO3 nanoparticles facilitated by multiple mechanisms," *Journal of Applied Physics*, vol. 115, no. 17, p. 173507, 2014.

[23] Q. Lou, X. Shi, X. Ruan et al., "Ferroelectric properties of Li-doped $BaTiO_3$ ceramics," *Journal of the American Ceramic Society*, vol. 101, no. 8, pp. 3597–3604, 2018.

[24] L. G. Devi and G. Krishnamurthy, "TiO_2- and $BaTiO_3$-assisted photocatalytic degradation of selected chloroorganic compounds in aqueous medium: correlation of reactivity / orientation effects of substituent groups of the pollutant molecule on the degradation rate," *The Journal of Physical Chemistry. A*, vol. 115, no. 4, pp. 460–469, 2011.

[25] C. Ponraj, G. Vinitha, and J. Daniel, "A review on the visible light active $BiFeO_3$ nanostructures as suitable photocatalyst in the degradation of different textile dyes," *Environmental Nanotechnology, Monitoring & Management*, vol. 7, pp. 110–120, 2017.

[26] L. H. Bac, L. T. H. Thanh, N. Van Chinh et al., "Tailoring the structural, optical properties and photocatalytic behavior of ferroelectric Bi 0.5 K 0.5 TiO 3 nanopowders," *Materials Letters*, vol. 164, pp. 631–635, 2016.

[27] F. Yang, L. Yang, C. Ai et al., "Tailoring bandgap of perovskite $BaTiO_3$ by transition metals co-doping for visible-light photoelectrical applications: a first-principles study," *Nanomaterials*, vol. 8, no. 7, p. 455, 2018.

[28] M. Otoničar, S. D. Škapin, B. Jančar, R. Ubic, and D. Suvorov, "Analysis of the Phase Transition and the Domain Structure in K0.5Bi0.5TiO3 Perovskite Ceramics by In Situ XRD and TEM," *Journal of the American Ceramic Society*, vol. 93, no. 12, pp. 4168–4173, 2010.

[29] D. D. Dung, D. V. Thiet, D. Odkhuu, L. V. Cuong, N. H. Tuan, and S. Cho, "Room-temperature ferromagnetism in Fe-doped

wide band gap ferroelectric $Bi_{0.5}K_{0.5}TiO_3$ nanocrystals," *Materials Letters*, vol. 156, pp. 129–133, 2015.

[30] S. Pigeot-Rémy, F. Simonet, E. Errazuriz-Cerda, J. C. Lazzaroni, D. Atlan, and C. Guillard, "Photocatalysis and disinfection of water: identification of potential bacterial targets," *Applied Catalysis B: Environmental*, vol. 104, no. 3-4, pp. 390–398, 2011.

[31] M. Nayak and M. R. Panigrahi, "Electron density calculation and structural analysis of $Li_{0.5}Bi_{0.5}TiO_3$ ceramic," *Advances in Applied Science Research*, vol. 6, no. 4, pp. 89–94, 2015.

[32] D. L. Wood and J. Tauc, "Weak absorption tails in amorphous semiconductors," *Physical Review B*, vol. 5, no. 8, pp. 3144–3151, 1972.

[33] H. S. Kushwaha, A. Halder, D. Jain, and R. Vaish, "Visible light-induced photocatalytic and antibacterial activity of Li-doped $Bi_{0.5}Na_{0.45}K_{0.5}TiO_3$–$BaTiO_3$ ferroelectric ceramics," *Journal of Electronic Materials*, vol. 44, no. 11, pp. 4334–4342, 2015.

[34] A. Houas, H. Lachheb, M. Ksibi, E. Elaloui, C. Guillard, and J. Herrmann, "Photocatalytic degradation pathway of methylene blue in water," *Applied Catalysis B: Environmental*, vol. 31, no. 2, pp. 145–157, 2001.

[35] H. Lachheb, E. Puzenat, A. Houas et al., "Photocatalytic degradation of various types of dyes (Alizarin S, Crocein Orange G, methyl red, Congo red, methylene blue) in water by UV-irradiated titania," *Applied Catalysis B: Environmental*, vol. 39, no. 1, pp. 75–90, 2002.

[36] H. H. Mohamed and D. W. Bahnemann, "The role of electron transfer in photocatalysis: fact and fictions," *Applied Catalysis B: Environmental*, vol. 128, pp. 91–104, 2012.

[37] D. Jain, H. K. Daima, S. Kachhwaha, and S. L. Kothari, "Synthesis of plant-mediated silver nanoparticles using papaya fruit extract and evaluation of their anti microbial activities," *Digest Journal of Nanomaterials and Biostructures*, vol. 4, no. 3, pp. 557–563, 2009.